Molecular Biology of the Cell
Vol. 20, 3700–3712, August 15, 2009

Rac1 Modulates Stimulus-evoked Ca^{2+} Release in Neuronal Growth Cones via Parallel Effects on Microtubule/Endoplasmic Reticulum Dynamics and Reactive Oxygen Species Production

Xiao-Feng Zhang and Paul Forscher

Department of Molecular, Cellular, and Developmental Biology, Yale University, New Haven CT 06520

Submitted July 16, 2008; Revised June 19, 2009; Accepted June 22, 2009
Monitoring Editor: Erika Holzbaur

The small G protein Rac regulates cytoskeletal protein dynamics in neuronal growth cones and has been implicated in axon growth, guidance, and branching. Intracellular Ca^{2+} is another well known regulator of growth cone function; however, effects of Rac activity on intracellular Ca^{2+} metabolism have not been well characterized. Here, we investigate how Rac1 activity affects release of Ca^{2+} from intracellular endoplasmic reticulum (ER) stores stimulated by application of serotonin (5-hydroxytriptamine). We also address how Rac1 effects on microtubule assembly dynamics affect distribution of Ca^{2+} release sites. Multimode fluorescent microscopy was used to correlate microtubule and ER behavior, and ratiometric imaging was used to assess intracellular Ca^{2+} dynamics. We report that Rac1 activity both promotes Ca^{2+} release and affects its spatial distribution in neuronal growth cones. The underlying mechanism involves synergistic Rac1 effects on microtubule assembly and reactive oxygen species (ROS) production. Rac1 activity modulates Ca^{2+} by 1) enhancing microtubule assembly which in turn promotes spread of the ER-based Ca^{2+} release machinery into the growth cone periphery, and 2) by increasing ROS production which facilitated inositol 1,4,5-trisphosphate-dependent Ca^{2+} release. These results cast Rac1 as a key modulator of intracellular Ca^{2+} function in the neuronal growth cone.

INTRODUCTION

The small G protein Rac plays a pivotal role in establishing cell polarity and controlling cell migration (Etienne-Manneville and Hall, 2002; Jaffe and Hall, 2005). Although Rac was initially characterized as a regulator of actin network assembly in lamellipodia of motile cells (Hall, 1998), later studies demonstrated that Rac has remarkable functional diversity. For example, Rac activation promotes microtubule assembly in epithelial cells (Wittmann *et al*., 2003, 2004) and the Rac activator DOCK7 inactivates the microtubule-destabilizing protein stathmin/Op18 in nascent axons (Watabe-Uchida *et al*., 2006). In addition, Rac is an essential component of NADPH oxidase complexes that produce reactive oxygen species (ROS) used for oxidative killing by phagocytes and for cellular signaling by nonmyeloid cells (Lambeth, 2004; Bedard and Krause, 2007). In neurons, genetic approaches suggest Rac is required for axon outgrowth, guidance, and branching (Luo, 2000; Guan and Rao, 2003); however, the underlying cell biological mechanisms are not yet well characterized.

Intracellular Ca^{2+} is another well known regulator of growth cone motility (Henley and Poo, 2004; Gomez and Zheng, 2006); however, Ca^{2+} effects on growth cone behavior seem to be pleiotropic. For example, in some cases Ca^{2+} increases induce growth cone collapse and inhibit neurite outgrowth (Cohan and Kater, 1986; Cohan *et al*., 1987; Mattson and Kater, 1987; Gomez *et al*., 1995, 2001; Gomez and Spitzer, 1999), but in others Ca^{2+} increases are correlated with filopodium protrusion and neurite elongation (Connor, 1986; Bedlack *et al*., 1992; Garyantes and Regehr, 1992; Lau *et al*., 1999; Cheng *et al*., 2002). Several lines of evidence indicate that Ca^{2+} regulates cytoskeletal function via Rac activation (Fleming *et al*., 1999; Price *et al*., 2003; Jin *et al*., 2005); in contrast, the inverse scenario, i.e., how Rac activity affects Ca^{2+} metabolism has not been well characterized.

Here, we address this question in the context of Ca^{2+} responses stimulated by application of the neurotransmitter serotonin (5-hydroxytryptamine, 5-HT) to neuronal growth cones. Specifically, we investigated how Rac effects on microtubule assembly and/or ROS production affect stimulus evoked Ca^{2+} release. We report that Rac1 activity promoted microtubule assembly-dependent endoplasmic reticulum (ER) advance which in turn resulted in spread of ER based Ca^{2+} release sites to the growth cone periphery. In parallel with these effects, Rac1 activity promoted ROS production in growth cones which facilitated 1,4,5-trisphosphate (IP_3)-dependent Ca^{2+} release in response to 5-HT application.

This article was published online ahead of print in *MBC in Press* (http://www.molbiolcell.org/cgi/doi/10.1091/mbc.E08–07–0730) on July 1, 2009.

Address correspondence to: Paul Forscher (paul.forscher@yale.edu).

MATERIALS AND METHODS

Cell Culture and Chemicals

Primary culture of *Aplysia* bag cell neurons as described previously (Forscher *et al*., 1987). 5-HT, U73122, U73343, Xestospongin C (XeC), ryanodine (Rya), Taxol, H_2O_2, and *N*-acetyl-cysteine (NAC) were from Sigma-Aldrich (St. Louis, MO). Heparin sodium salt, vinblastine, apocynin, genistein, and ionomycin were from Calbiochem (San Diego, CA). L61 Rac1-glutathione-S-transferase (GST) and N17 Rac1-GST, referred to here as "CA Rac1" and "DN Rac1", respectively, were from Cytoskeleton (Denver, CO), and biological activity of these constructs was confirmed by the manufacturer. Calcium Green-1 dextran, potassium salt, 3000 molecular weight (MW) (CG-1), Texas

Red dextran, 3000 MW (Texas Red), BODIPY FL brefeldin A and CM-H2DCFDA (DCF) were purchased from Invitrogen (Carlsbad, CA). Anti-KDEL antibody MAC 256 was from Abcam (Cambridge, MA).

Solutions

Artificial seawater (Na-ASW) contained 400 mM NaCl, 10 mM KCl, 15 mM HEPES, 10 mM $CaCl_2$, and 55 mM $MgCl_2$ at pH 7.8. Na-AWS supplemented with 3 mg/ml bovine serum albumin (BSA), 0.5 mM vitamin E (Sigma-Aldrich), and 1 mg/ml carnosine (Sigma-Aldrich) before experiments. Ca^{2+}-free ASW was as for Na-ASW except that $CaCl_2$ is omitted and EGTA (0.5 mM) is included. Ca^{2+} injection buffer consisted of 100 mM potassium aspartate and 10 mM HEPES at pH 7.4.

Microinjection

Microinjection protocol as described previously (Lin and Forscher, 1995). For Ca^{2+} imaging, neurons were injected with CG-1 and Texas Red in Ca^{2+} injection buffer (needle concentration 11–15 and 0.3–0.4 mg/ml, respectively). For microtubule dynamics, neurons were injected with 1 mg/ml Alexa-Fluor 594-labeled tubulin. To generate CA and DN Rac1 backgrounds: L61 Rac1-GST (CA Rac1) or N17 Rac1-GST (DN Rac1) was included in the injection needle (concentration 0.7–1.0 mg/ml) as described previously (Zhang *et al*., 2003), along with tubulin probes or Texas Red volume tracer with or without Ca^{2+} dye. For ROS assays, neurons were injected with 0.4 mg/ml Texas Red as a volume tracer. Reagent or vehicle solution injections were typically ~10% of cell volume. After microinjection, cells were incubated in Na-ASW 1 h before imaging.

Ca^{2+} Imaging and Analysis

Fluorescence images of growth cones loaded with Ca^{2+} dye CG-1 and Texas Red volume tracer were obtained using an Eclipse TE300 microscope (Nikon, Tokyo, Japan) equipped with a Quantix 57 back-illuminated frame transfer cooled charge-coupled device camera (Photometrics, Tucson, AZ) mounted on the bottom port. Similar Ca^{2+} profiles and dynamics were observed in control experiments using 70,000 MW CG-1 ruling out the possibility that the 3,000 MW CG-1 used here could be portioning into intracellular stores. Two programmable fast filter wheels (100-ms filter changes) that include shutters were mounted with bandpass filters (Ludl,) for changing both excitation and emission wavelengths. Fluorescence filters used (denoted as center wavelength/bandwidth) were as follows: CG-1: 484/15 nm for excitation, and 523/15 nm for emission; Texas Red: 555/25 nm for excitation and 605/25 nm for emission (Chroma Technology, Brattleboro, VT). Paired images with comparable intensities of CG-1 and Texas Red were recorded every 10 or 20 s by using 400- to 600-ms integration times for fluorescein isothiocyanate (FITC) channel (Ca^{2+} signal) and 100- to 200-ms integration times for fluorescein isothiocyanate (TRITC) channel (volume signal). The ratio images (CG-1/Texas Red) were created by dividing background corrected intensity values of CG-1 fluorescence by Texas Red fluorescence and then converted into time-lapse montages or kymograph for data analysis. Average pixel intensity values were obtained from the entire C-domain and P-domain (see Figure 1D) of the growth cones of interest. Ca^{2+} changes over time were expressed as $\Delta F/F_0$, where $\Delta F = F_t - F_0$ and F_0 was the average Ca^{2+} level sampled during ~3- to 5-min baseline period (before 5-HT addition). $\Delta F/F_o$ (%) greater than 10% was considered significant. Ten- or 20-s sampling intervals were used for Ca^{2+} imaging. This sampling regime would not resolve Ca^{2+} transients with <1-s time constants such as observed in *Xenopus* growth cones (Gomez *et al*., 2001) and thus does not address potential contributions of these events.

To assess basal Ca^{2+} levels in growth cones, ratiometric Ca^{2+} images were performed first in Na-ASW to get basal fluorescence ratio. Subsequently, the bath solution was exchanged with Ca^{2+}-free AWS with addition of various concentrations of $CaCl_2$ (~0.1–0.4 mM) to yield free Ca^{2+} concentration ranging from ~45 to 720 nM (WEBMAXCLITE, http://www.stanford.edu/~cpatton/webmaxc/webmaxclite115.htm). Ionomycin (10 μM) was included to equilibrate extracellular and intracellular Ca^{2+} levels. The fluorescence ratio acquired in each corresponding bath solution was normalized to the basal fluorescence ratio. The graph of normalized fluorescence ratio (percentage) plotted against free Ca^{2+} concentration exhibited a linear regression with $R^2 > 0.96$.

Actin and Microtubule Immunocytochemistry

Bag cell neurons were fixed by rapid exchange of the medium with 3.7% formaldehyde in ASW supplemented with 400 mM sucrose. After fixation for 20 min, the cells were permeabilized for 5 min using 1% Triton X-100 in the fixation solution. Cells were then washed three times with phosphate-buffered saline (PBS) containing 0.1% Triton X-100 (wash solution). For actin filament labeling, Alexa 594-phalloidin (Invitrogen) was incubated at 1:50 in wash solution for 1 h. After three washes, the cells were blocked with 5% BSA in wash solution for 30 min and then incubated with mouse anti-α-tubulin (Sigma-Aldrich) at 1:100 in blocking solution for 30 min at room temperature (RT). After three washes, Alexa 488-goat anti-mouse immunoglobulin G (IgG) (Invitrogen) was added at 1:100 in blocking solution for 30 min at RT. The final wash solution was replaced with anti-fading solution Mowiol (Calbiochem, San Diego, CA). Microtubules and actin filaments were visualized using the same filters as CG-1 and Texas Red as described above.

ER Immunocytochemistry

An anti-KDEL antibody was used to visualize ER structure (Munro and Pelham, 1987; Saunders and Cohen, 1999). Cells were fixed with 4% paraformaldehyde for 15 min, permeabilized with 0.5% Triton X-100 for 5 min, and then incubated with 5% BSA and 10% normal goat serum for 1 h. After blocking, cells were stained with rat anti-KDEL antibody (MAC 256; diluted 1:100) for 1 h and visualized with Alexa 594-goat anti-rat IgG (Invitrogen) for 30 min. ER distribution and actin filaments (labeled with Alexa 488-phalloidin) were visualized in growth cones by spinning disk confocal microscopy (Andor, Belfast, Northern Ireland). Alexa 488 and Alexa 594 were excited simultaneously with 488 and 561 nm laser lines, and emission was monitored using 535/40 nm and 625/40 nm filters respectively (Chroma Technology).

ER Vital Labeling

BODIPY FL brefeldin A was used for ER staining (Deng *et al*., 1995; Cifuentes *et al*., 2001). Neurons were labeled in Na-ASW containing BODIPY FL brefeldin A (2 μM) in total darkness for 30 min. At the end of the incubation period, cells were extensively washed and mounted in a laminar flow chamber for observation. In most cases, neurons were injected with CA Rac1 or DN Rac1. For visualizing microtubule and ER simultaneously, microtubule probe was also injected beforehand. The fluorescence filters used for the ER and microtubule imaging were the same as for CG-1 and Texas Red as described above.

ROS Detection

CM-H2DCFDA (DCF) was used for ROS detection (Xie *et al*., 1999). Neurons injected with Texas Red were loaded with DCF (40 μM) for 1.5 h in the dark in Na-ASW and then washed thoroughly. Fifteen minutes later the coverslip was affixed to a chamber for visualization. In most cases, neurons were also injected with CA Rac1 or DN Rac1. The filter settings for the volume corrected ROS imaging were the same as for CG-1 and Texas Red as described above. Paired images of DCF and Texas Red were recorded using 200-to 500-ms integration times for FITC channel (ROS signal) and 100- to 200-ms integration times for TRITC channel (volume signal). The path length corrected image was generated by dividing background subtracted pixel values of DCF fluorescence by those of Texas Red fluorescence. To verify the sensitivity of this assay, a line scan in ROS kymograph derived from DCF/Texas Red images was done during H_2O_2 (10 μM) exposure. To quantify ROS levels, the values of DCF/Texas Red in C-domain and P-domain were measured in different Rac1 backgrounds and plotted as box-whisker plots.

Quantitative Analysis

Microtubule and ER dynamics assessed by fluorescent speckle microscopy (FSM) a technique for direct quantitative assessment of cytoskeletal polymer dynamics in living cells (Waterman-Storer *et al*., 1998; Waterman-Storer and Salmon, 1998b). Multimode time lapse microscopy as described previously (Schaefer *et al*., 2002). In brief, three-channel recordings were made every 12 s by using 300- to 700-ms integration times for microtubules, 100 to 400 ms for ER visualization, and 50 ms for differential interference contrast (DIC) images. Microtubule dynamic parameters were assessed as reported previously (Schaefer *et al*., 2002). To quantify ER density and advance, the P-domain was divided into quartiles starting at the C–P-domain interface and ending at the leading edge (see Figure 1D). Microtubule/ER excursions were quantified by counting the number of microtubules or ER tubules spanning 25 or 75% of the P-domain (denoted 25%P or 75%P, respectively). ER–microtubule-coupling efficiency was estimated by dividing ER by microtubule excursions assessed at the same time. Data are expressed as mean ± SEM, unless stated otherwise. Statistical analysis was done with two tailed paired or unpaired *t* test.

RESULTS

Rac1 Promotes Microtubule–ER Advance into P-Domain

Given that Rac1 activity can promote microtubule assembly in nonneuronal cells (Wittmann *et al*., 2003), we first characterized microtubule dynamics in different Rac1 activity backgrounds by using FSM as described previously (Schaefer *et al*., 2002) (also see Supplemental Figure S1). Growth cones are composed of two distinct cytoplasmic domains: 1) the central or C-domain, characterized by fast organelle transport and high microtubule density; and 2) the peripheral or P-domain, consisting of dense dynamic actin networks that tend to exclude organelles larger than ~50 nm (Figure 1D; Forscher *et al*., 1987).

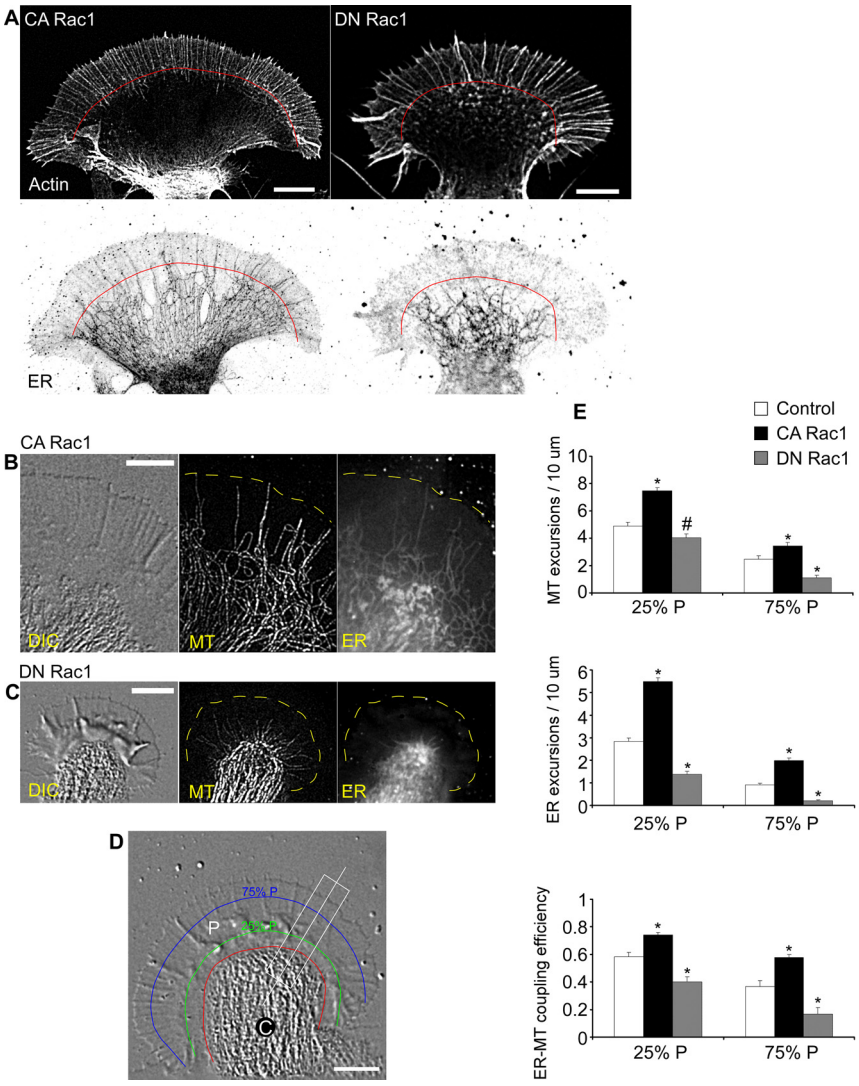

Figure 1. Rac1 promotes microtubule–ER advance into P-domain. (A) Immunocytochemistry of actin filament and ER distribution in a growth cone in CA Rac1 backgrounds (left) or DN Rac1 backgrounds (right). Top, actin. Bottom, ER. Red line, filopodial ends. Bar, 10 μm. (B) Simultaneous labeling of microtubule and ER in CA Rac1 injected neuron. From left to right, DIC, microtubule and ER. Bar, 10 μm. (C) As in B in DN Rac1-injected neurons. (D) DIC image indicating C- and P-cytoplasmic domains and reference lines used in calculating ER and microtubule excursion numbers (see *Materials and Methods*). C, C-domain; P, P-domain. Red line, interface between C-domain and P-domain defined by organelle boundary; green line, 25%P; blue line, 75%P. Bar, 10 μm. (E) Quantification of microtubule versus ER excursions past 25%P and 75%P boundaries in control, CA Rac1, or DN Rac1. Top, microtubule excursion number; middle, ER excursion number; and bottom, ER—microtubule-coupling efficiency. Data between growth cones normalized by boundary length. N = 10 (control), 12 (CA Rac1), and 8 (DN Rac1) for microtubule excursion assay; N = 16 (control), 14 (CA Rac1), and 12 (DN Rac1) for ER excursion assay; and N = 9 (control), 10 (CA Rac1), and 8 (DN Rac1) for ER—microtubule-coupling efficiency assay. N denotes the number of growth cones tested. Values are expressed as mean ± SEM. Statistical analysis by two-tailed unpaired *t* test. *$p < 0.01$ versus control and #$p < 0.05$ versus control.

We found that constitutively active (CA) Rac1 increased microtubule rescue frequency by 160% and decreased catastrophe frequency by −28% in the P-domain (Table 1). Dominant-negative (DN) Rac1 had the opposite effect: decreasing microtubule rescue frequency and increasing microtubule catastrophe frequency in the P-domain by −32 and 200%, respectively (Table 1). As a result, microtubules tended to spend a greater proportion of the time growing and relatively less time shrinking in CA Rac1 compared with DN Rac1 backgrounds. Absolute microtubule growth and shortening velocities did not seem to be significantly affected by Rac1 activity. It is important that more persistent microtubule growth in the presence of CA Rac1 promoted deep microtubule advances into the P-domain, consistent with previous observations in epithelial cells (Wittmann *et al.*, 2003).

We next examined the effect of Rac1 activity on ER distribution in the growth cones by using an anti-KDEL antibody to visualize ER distribution and Alexa-phalloidin to locate characteristic cytoplasmic domains in fixed cells (Saunders

Table 1. Microtubule dynamic parameters as a function of Rac1 background activity

Condition	Rescue frequency (/min)	Catastrophe frequency (/min)	% time growing	% time paused	% time shortening	Growth velocity (μm/min)	Shortening velocity (μm/min)
Control	1.54 ± 0.10	0.96 ± 0.07	41.2 ± 2.1	23.0 ± 1.9	35.8 ± 2.1	6.50 ± 0.54	−9.01 ± 0.94
CA Rac1	4.01 ± 0.22*	0.69 ± 0.04*	59.4 ± 1.7*	23.8 ± 1.9	16.8 ± 1.1*	6.55 ± 0.35	−8.66 ± 0.74
DN Rac1	1.04 ± 0.06*	2.86 ± 0.23*	16.2 ± 1.7*	19.4 ± 2.4	64.4 ± 1.6*	6.46 ± 0.61	−7.94 ± 0.85

Plus-end periphery microtubules: control (n = 25 microtubules), CA Rac1 (n = 31 microtubules), and DN Rac1 (n = 25 microtubules). Mean ± SEM elapsed recording time: 3–5 min. *$p < 0.001$ vs. control.

and Cohen, 1999). In CA Rac1 backgrounds, the ER tended to splay out in the growth cone with projections deep into the P-domain (Figure 1A, bottom left). In contrast, in DN Rac1 backgrounds, the ER was restricted to the C-domain (Figure 1A, bottom right). Under control conditions, we observed an intermediate phenotype with some ER tubules extending into the periphery (Supplemental Figure S2).

Given that ER distribution is dynamically regulated by microtubule-based transport in neuronal growth cones (Dailey and Bridgman, 1989, 1991) and other motile cells (Terasaki *et al*., 1986; Waterman-Storer and Salmon, 1998a), we next co-visualized microtubule and ER dynamics in the growth cone by FSM and BODIPY brefeldin-A imaging (Deng *et al*., 1995; Cifuentes *et al*., 2001). In CA Rac1 backgrounds, growth cones tended to have well spread C-domains with microtubules and ER both extending deep into the P-domain (Figure 1B and Supplemental Movie 1). In contrast, in DN Rac1 backgrounds, growth cones tended to have more compact, focused C-domains (Figure 1C). Although microtubules still sometimes extended into the P-domain, the ER did not enter the P-domain nearly as efficiently (Figure 1C and Supplemental Movie 2). Note that individual images tend to underestimate the time-averaged density of the ER in the P-domain because peripheral ER is associated with a highly dynamic population of microtubules (Schaefer *et al*., 2002; Suter *et al*., 2004).

To quantify these Rac effects, we counted microtubule and ER excursions past fiducial marks placed at 25 and 75% of

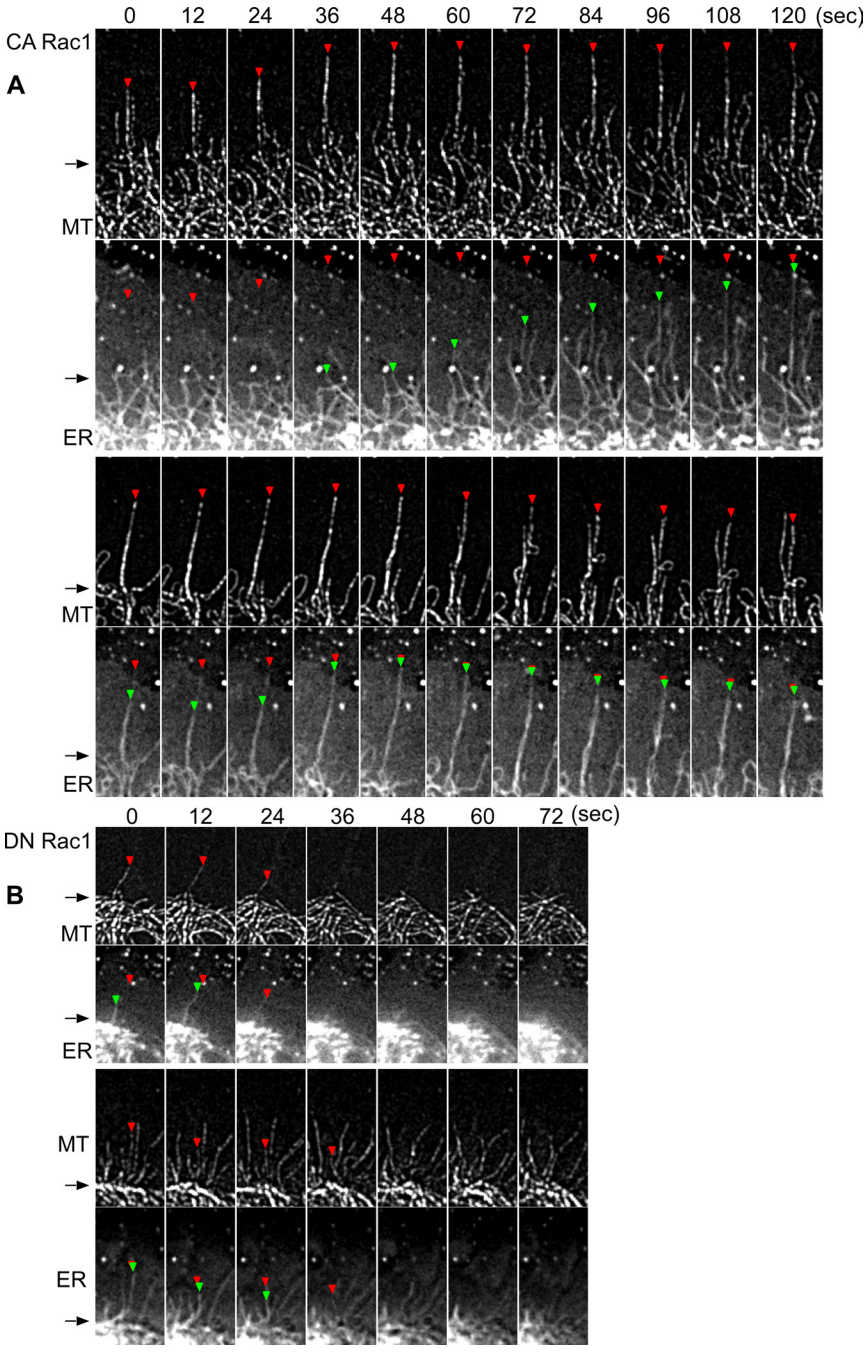

Figure 2. Rac1 alters ER dynamic behavior on microtubules. (A) Two representative examples of time-lapse sequences of microtubule (top) and ER (bottom) in CA Rac1 backgrounds. Red and green arrowheads point to microtubule and ER tips, respectively. Note that the red arrowheads in ER panel indicate the corresponding position of microtubule tips. Elapsed time (seconds) is shown at the top. Arrows denote position transition zone between C- and P-domains. (B) DN Rac1 background. Regions are similar to white box in Figure 1D.

the width of the P-domain under all conditions (Figure 1D, green 25%P, blue 75%P lines, respectively; see *Materials and Methods*). The number of microtubule and ER excursions past the 25%P and 75%P marks increased in CA Rac1 and decreased in DN Rac1 backgrounds relative to controls (Figure 1E, top and middle, respectively). We also calculated the ratio of ER to microtubule excursions to estimate ER–microtubule-coupling efficiency, and found that CA Rac1 significantly increased this ratio in both the proximal (25%P) and distal (75%P) regions of the P-domain relative to controls, whereas DN Rac1 had the opposite effect (Figure 1E, bottom).

A detailed analysis of microtubule versus ER dynamics in CA versus DN Rac1 backgrounds is shown in Figure 2. Distal microtubule and ER ends are denoted by red and green triangles, respectively. Under both conditions, microtubule ends could enter the P-domain without ER attached; however, ER was never found in the periphery without a microtubule present. CA Rac1 dramatically increased microtubule rescue frequency, resulting in microtubules spending more time growing (Table 1) which in turn promoted ER advance. Figure 2A shows an example of ER extending outward along what seems to be a previously assembled microtubule. However, it is difficult to distinguish between ER elongating along a microtubule versus ER tracking with a microtubule tip (Grigoriev *et al.*, 2008) because microtubules can coalign, making unambiguous plus-end localization challenging. An example of two closely aligned microtubules separating is evident in the 48- to 72-s interval in Figure 2A, bottom. Colabeling microtubules with a microtubule tip-tracking protein such as EB3 will be needed to resolve this issue.

In contrast, increased microtubule catastrophe frequencies were observed in DN Rac1 (Table 1). This resulted in shorter

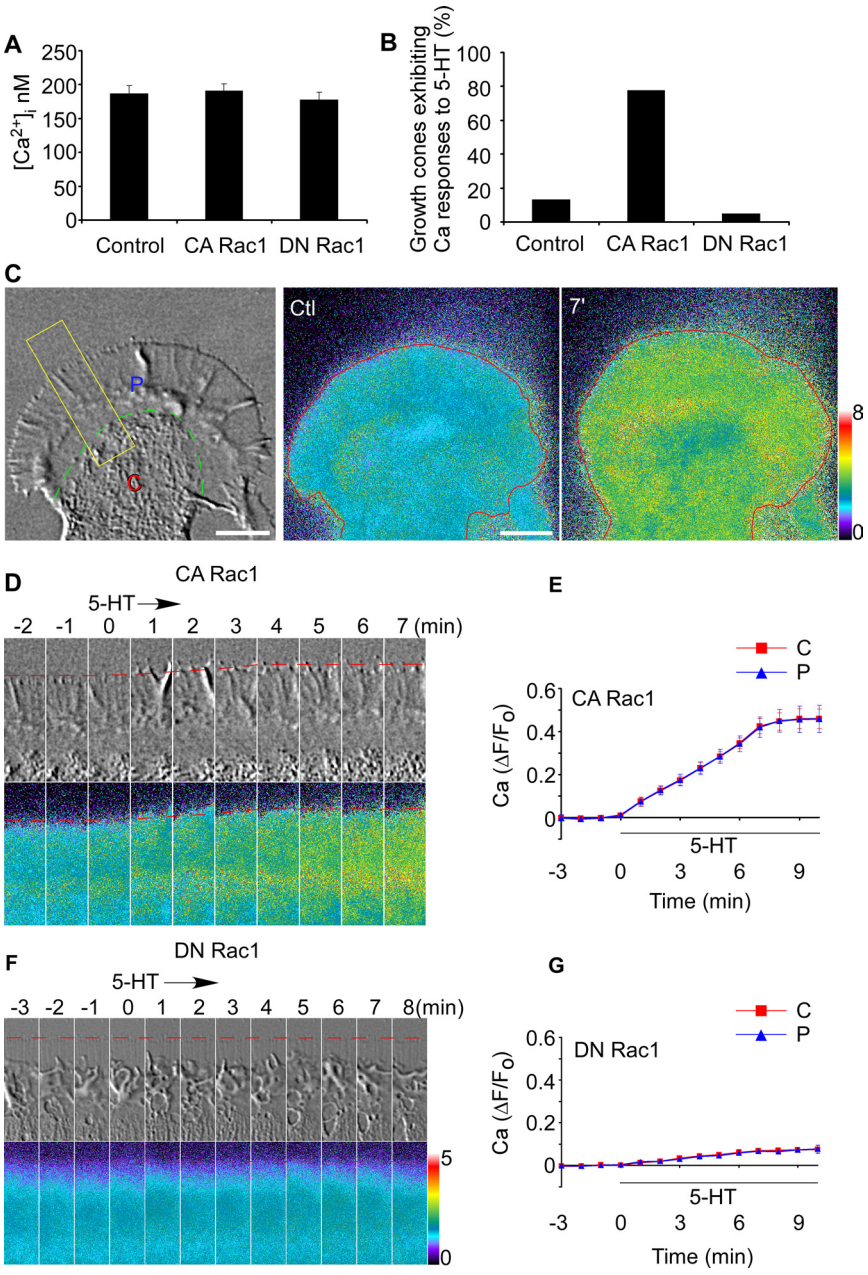

Figure 3. 5-HT evokes Ca^{2+} rise in CA Rac1 backgrounds. (A) Baseline Ca^{2+} level in growth cones in different Rac1 backgrounds. N = 6 (control), 6 (CA Rac1), or 5 (DN Rac1). Values are expressed as mean ± SEM. (B) Probability of 5-HT (10 μM)-evoked Ca^{2+} responses in growth cones in control, CA Rac1-, or DN Rac1-injected neurons. N = 15 (control), 18 (CA Rac1), or 20 (DN Rac1). (C) Left, DIC image of growth cone. C, central domain (C-domain); P, peripheral domain (P-domain). Green dashed line, interface between C-domain and P-domain defined by organelle boundary. Middle and right, Ca^{2+} ratio images of the entire growth cone before (ctl) and after 7 min in 5-HT (10 μM throughout). Red line, leading edge. Bar, 10 μm. (D and F) Time course of 5-HT (10 μM) effects. DIC (top) and Ca^{2+} ratio images (bottom) in CA Rac1- (D) or DN Rac1 (F)-injected neuron obtained from area of interest as indicated in C (left, yellow rectangle). Elapsed time (minutes) is shown at the top. Red dotted line, peripheral boundary. (E and G) Summary of $\Delta F/F_0$ plots recorded in the entire C-domain (red line) or P-domain (blue line) of growth cones quantifying Ca^{2+} response to 5-HT over time in CA Rac1 (E) or DN Rac1 (G) backgrounds. N = 5 (CA Rac1) or 4 (DN Rac1). Values are expressed as mean ± SEM. Black bar shows 5-HT presence. N denotes the number of growth cones tested. Ca^{2+} ratio image is coded by pseudocolors in linear scale (see bars).

average microtubule growth periods and consequent ER depletion from the P-domain (Figure 2B).

Rac1 Regulates the Probability of 5-HT–evoked Ca^{2+} Elevation

5-HT has both neurotransmitter and neuromodulator roles in neuronal development (Gaspar *et al.*, 2003). Because *Aplysia* 5-HT receptors have been extensively characterized previously (Li *et al.*, 1995; Barbas *et al.*, 2005), and Ca^{2+} has been reported to participate in 5-HT function in neurons (Dropic *et al.*, 2005; Li *et al.*, 2005), we investigated whether Rac1 activity might affect 5-HT-evoked Ca^{2+} responses. We first tested the effect of Rac1 activity on basal Ca^{2+} levels and no significant differences were observed in different Rac1 backgrounds (Figure 3A).

Next, Ca^{2+} responses to 5-HT were assessed. Under control conditions only 13% of growth cones tested exhibited Ca^{2+} increases after 5-HT application (Figure 3B), and these responses tended to be transient. It is interesting that when cells were injected with CA Rac1, nearly 80% of growth cones tested responded to 5-HT with Ca^{2+} increases (Figure 3B and Supplemental Movie 3). A representative response in CA Rac1 background is shown in Figure 3, C and D. 5-HT triggered a sustained increase in Ca^{2+} in the entire growth cone, including C- and P-domains. After 5-HT washout, Ca^{2+} returned to baseline levels in 30–40 min (data not shown). Ca^{2+} response curves over time in C-domain and P-domain were essentially indistinguishable, reaching plateau levels after 7–8 min in 5-HT with a maximal increase of 45% (Figure 3E).

In contrast, in DN Rac1 backgrounds 5-HT typically did not trigger significant Ca^{2+} changes, and the response probability was only 5% (Figure 3, B, F, and G). Brief Ca^{2+} transients (<1 min in duration) were sometimes observed in the axon shaft in DN Rac1 backgrounds; however, these events were not counted as positive responses because they did not affect Ca^{2+} levels in C- or P-domains. Together, these results suggest that Rac1 activity increases the probability

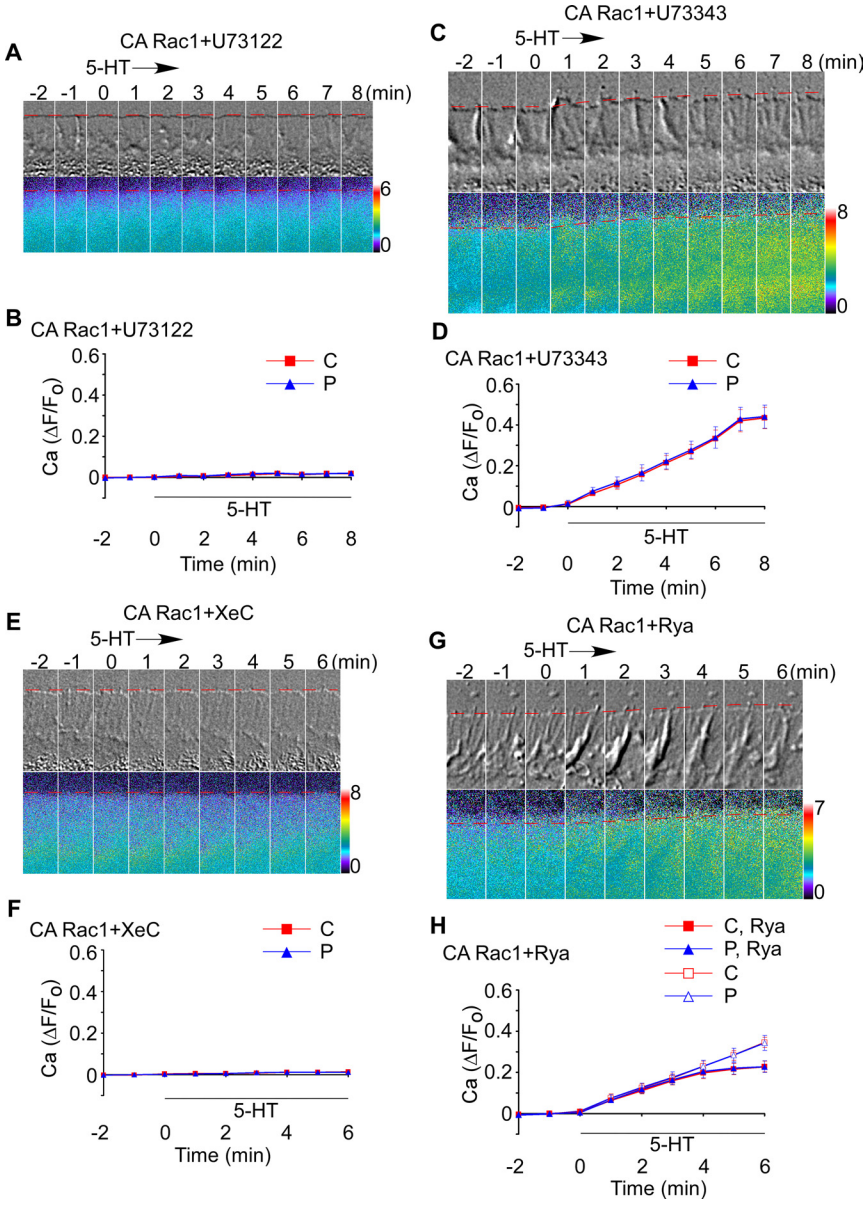

Figure 4. 5-HT–evoked Ca^{2+} rise depends on PLC→IP_3 signaling cascade. (A and C) Time-lapse montage of DIC (top) and Ca^{2+} ratio imaging (bottom) during 5-HT (10 μM) treatment in CA Rac1-injected neurons pretreated with U73122 (2 μM) (A) or U73343 (2 μM) (C) for 30 min. (E and G) Time-lapse sequence of DIC (top) and Ca^{2+} ratio imaging (bottom) during 5-HT (10 μM) exposure in CA Rac1-injected neurons pretreated with XeC (20 μM) for 30 min (E) or Rya (25 μM) for 40 min (G). Dotted line, peripheral boundary. Elapsed time is shown at the top of DIC in minutes. Ca^{2+} ratio image is coded by pseudocolors in linear scale (see bars). B, D, F, and H, summary of $\Delta F/F_0$ plots recorded in the entire C-domain (red line) or P-domain (blue line) of growth cones quantifying Ca^{2+} response to 5-HT over time in CA Rac1-injected neurons pretreated with U73122 (2 μM) (B), U73343 (2 μM) (D), or XeC (20 μM) (F) for 20–30 min or with Rya (25 μM) (H) for 40–50 min. In H, the control curves for C-domain and P-domain from Figure 3E are shown for comparison. Black bar shows 5-HT presence. N = 4 (CA Rac1 + U73122), 3 (CA Rac1 + U73343), 4 (CA Rac1 + XeC), or 4 (CA Rac1 + Rya). N denotes the number of growth cones tested. Values are expressed as mean ± SEM.

and amplitude of Ca^{2+} increases in response to 5-HT in the C- and P-domains of the growth cone.

5-HT-evoked Ca^{2+} Responses Involve Phospholipase C (PLC)→IP_3 Signaling

We next investigated the Rac1-dependent Ca^{2+} response mechanism. In many cell types, 5-HT activates PLC, leading to IP_3 formation and Ca^{2+} release from IP_3 receptors (Yoder *et al.*, 1996; Chiu *et al.*, 1999; Noda *et al.*, 2003; Dropic *et al.*, 2005; Li *et al.*, 2005). To investigate a role for PLC in 5-HT–induced responses, CA Rac1-injected neurons were pretreated for 30 min with U73122, a well known PLC inhibitor (Jin *et al.*, 1994; Zhou *et al.*, 1999), and Ca^{2+} imaging was performed before and after 5-HT exposure. PLC inhibition completely suppressed Ca^{2+} elevation in response to 5-HT (Figure 4, A and B). In control experiments using U73343, an inactive U73122 analog (Smith *et al.*, 1990; Jin *et al.*, 1994), 5-HT elicited typical Ca^{2+} responses (Figure 4, C and D), ruling out nonspecific U73122 effects. These results indicate that 5-HT-evoked Ca^{2+} responses depend on PLC activation. To investigate the role of IP_3 receptor activation, we assessed Ca^{2+} responses in the presence of the membrane-permeable IP_3 receptor blocker XeC (Gafni *et al.*, 1997). XeC pretreatment completely blocked 5-HT dependent Ca^{2+} release (Figure 4, E and F). Similar inhibition of 5-HT effects on Ca^{2+} release was observed when neurons were injected with heparin (Takei *et al.*, 1998)—a chemically distinct IP_3 receptor antagonist (data not shown).

We also tested whether Ca^{2+} release from ryanodine receptor (RyaR)-gated Ca^{2+} stores could be involved in the observed 5-HT responses. Ca^{2+} release from RyaR stores is activated by low concentrations (10–100 nM) and blocked by high concentrations (>10 μM) of ryanodine (Meissner, 1986; McPherson *et al.*, 1991); therefore, CA Rac1-injected neurons were treated with an inhibitory dose of ryanodine (25 μM) for 40 min and then exposed to 5-HT in the continued presence of the inhibitor. Under these conditions, 5-HT continued to evoke Ca^{2+} release (Figure 4G).

Although the early phase of the Ca^{2+} response was unaffected by ryanodine, Ca^{2+} responses plateaued at lower levels after ~5 min (Figure 4H). These results are consistent with Ca^{2+}-induced Ca^{2+} release from RyaR stores contributing mainly to the late phase of the 5-HT-elicited Ca^{2+} rise. Because the RyaR and the IP_3 receptors regulate a common ER-associated Ca^{2+} pool (Walton *et al.*, 1991; Solovyova and Verkhratsky, 2003), it is not surprising that IP_3 receptor activation could lead to further RyaR-dependent Ca^{2+} release. Together, these data strongly suggest CA Rac1 is

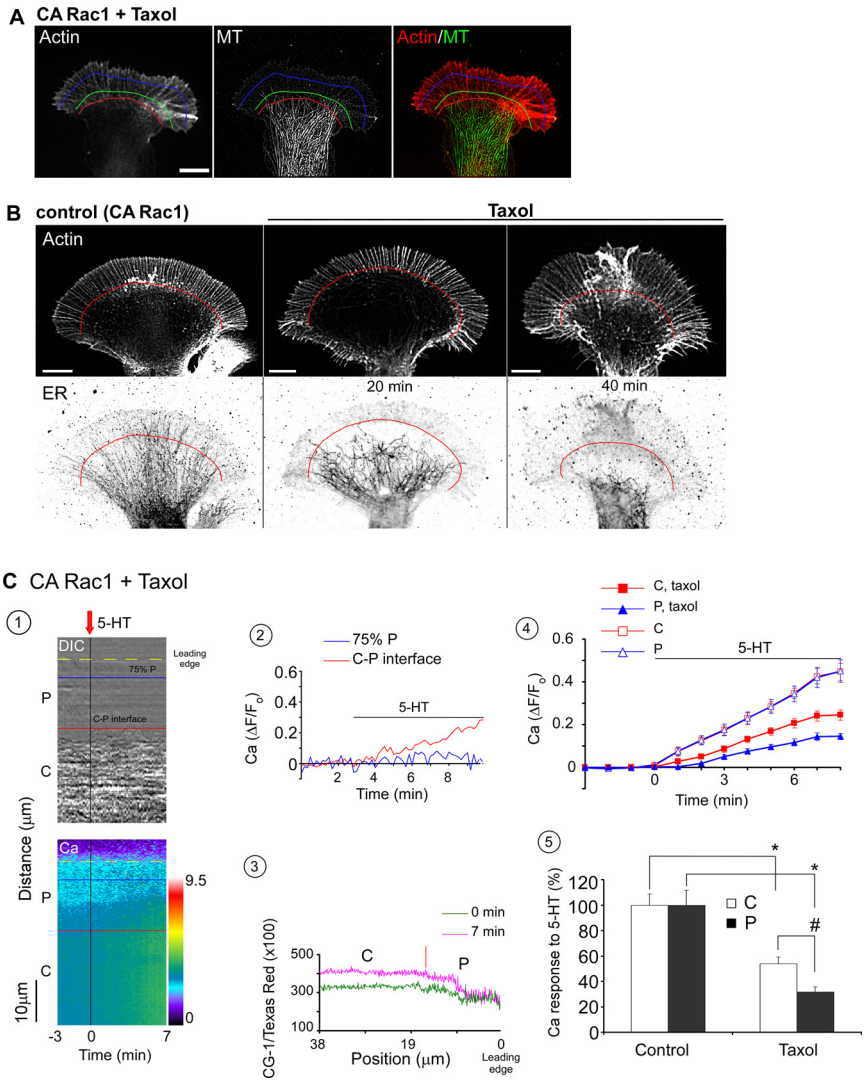

Figure 5. Rac1 effects on microtubule–ER distribution modulate the pattern of 5-HT–evoked Ca^{2+} release. (A) Immunocytochemistry of actin filament and microtubule distribution in a Taxol (0.1 μM; 20 min) pretreated growth cone in CA Rac1 backgrounds. Left, Actin. Middle, microtubule. Right, merge of actin filaments (red) and microtubules (green). Red, green, and blue lines: boundaries as in Figure 1D. Bar, 10 μm. (B) Taxol (0.1 μM) effects on ER distribution in growth cones in CA Rac1 backgrounds. Top, actin staining. Bottom, ER staining. Left, control. Middle, Taxol treatment for 20 min. Right, Taxol treatment for 40 min. Red line, C–P-domain boundary. Bar, 10 μm. (C) 5-HT–evoked Ca^{2+} release in a Taxol-pretreated (0.1 μM; 20 min) growth cone in CA Rac1 background. (1) DIC and Ca^{2+} kymographs sampled from a region similar to the white bar in Figure 1D before and after 5-HT (10 μM) addition. Note Taxol was present throughout. Data acquired at 10-s intervals. Blue line, 75%P; red line, C–P interface; yellow line, leading edge. P, P-domain; C, C-domain. Ca^{2+} kymograph is coded by pseudocolors in linear scale (see bar). (2) Time course of 5-HT–evoked Ca^{2+} response sampled from blue line and red line. (3) Ca^{2+} profiles sampled at 0 and 7 min showing Ca^{2+} distribution across growth cone. Red line indicates C–P-domain interface. (4) $\Delta F/F_0$ plots of 5-HT response recorded from entire C-domain (red) or P-domain (blue) of growth cones pretreated with Taxol (0.1 μM; 20–30 min). Control curves for C- and P-domains from Figure 3E are shown for comparison (open symbols). N = 5 growth cones for each condition. Values are expressed as mean ± SEM. Black bar shows 5-HT presence. (5) Comparison of 5-HT (10 μM) evoked peak Ca^{2+} for control versus Taxol (0.1 μM; 20–30 min) pretreated growth cones in CA Rac1 backgrounds. Data from entire C- or P-domains normalized to control conditions. N = 5 growth cones for each condition. Values are expressed as mean ± SEM. *$p < 0.01$ and #$p < 0.05$.

potentiating 5-HT–evoked Ca^{2+} release from IP_3- and ryanodine receptor-gated Ca^{2+} stores.

Ca^{2+} Release Topography Depends on Microtubule Assembly

The observation that CA Rac1 promoted microtubule and ER advance into the growth cone periphery (Figure 1, A, B, and E) suggested the possibility that Rac1 activity might spatially regulate Ca^{2+} release. To test this hypothesis, we used low levels of Taxol (100 nM) or vinblastine (25 nM) that damp microtubule assembly and have been shown to result in rapid clearance of microtubules from P-domain due to persistent microtubule coupling to retrograde actin flow (Suter *et al*., 2004). Taxol treatment would be expected to result in rapid ER clearance from the P-domain given ER coupling to microtubule movements (Figure 2).

We first assessed actin filament and microtubule distributions in CA Rac1-injected neurons with or without Taxol (0.1 μM; 20 min) treatment. In control growth cones, individual microtubules aligned with filopodia (Schaefer *et al*., 2002) and penetrated into the P-domain (Supplemental Figure S3); in contrast, microtubules rarely entered the P-domain at all in Taxol-treated growth cones (Figure 5A).

Next, we examined ER distribution before and after Taxol treatment in CA Rac1 backgrounds. Taxol treatment resulted in a dramatic relocalization of ER within the growth cone (Figure 5B and Supplemental Movie 4). Low levels of vinblastine that have similar effects on microtubule dynamics had similar effects on ER distribution (Supplemental Figure S4C). It is interesting that ER network density decreased in C-domain over time under these conditions, which could account for the decrease in C-domain Ca^{2+} responses observed. These results suggest microtubule presence alone (Figure 5A) is not sufficient to sustain Ca^{2+} release in the C-domain and point to a novel role for microtubule assembly considered in the *Discussion*.

To assess Taxol/vinblastine effects on ER distribution, we quantified ER excursion events in CA Rac1 backgrounds (Table 2). ER excursions past the 25%P domain boundary decreased by ~60% after Taxol or vinblastine addition and no ER extended past 75%P boundary (Table 2). These observations suggested that alteration in microtubule assembly could affect spatial patterns of Ca^{2+} release by causing redistribution of ER Ca^{2+} stores, especially in the growth cone P-domain.

To test this hypothesis, we assessed 5-HT-evoked Ca^{2+} release in CA Rac1 backgrounds after inhibition of microtubule dynamics with Taxol. Under these conditions, Ca^{2+} elevation was restricted to the C-domain and proximal region of the P-domain (Figure 5C1 and Supplemental Movie 5). Ca^{2+} levels no longer changed at all beyond the 75%P peripheral domain boundary (Figure 5C, 2 and 3) as observed under control conditions (compare Figure 3C). Figure 5C, 4 and 5, compares pooled control versus Taxol-pretreated 5-HT-evoked Ca^{2+} responses. C- and P-domain responses are of similar magnitude under control conditions; in contrast, Ca^{2+} responses were reduced in both the C- and P-domains after Taxol treatment (Figure 5C, 4 and 5) in accord with the observed reduction of ER density. Similar results were obtained using vinblastine (Supplemental Figure S4, A and B). Reduction of Ca^{2+} release in the C-domain subsequent to Taxol treatment was somewhat of a surprise because Taxol did not markedly alter microtubule density there (cf. Figure 5A). This finding bears further investigation as it suggests the possibility that a dynamic pool of microtubules in the C-domain may play a role in maintaining ER distribution there.

Table 2. Taxol/vinblastine changes ER distribution in growth cones in CA Rac1 background

Boundary	before Taxol	Taxol	before Vinblastine	Vinblastine
25%P	5.42 ± 0.17	2.32 ± 0.16*	5.36 ± 0.18	2.12 ± 0.25*
75%P	2.04 ± 0.16	0 ± 0*	1.97 ± 0.17	0 ± 0*

CA Rac1-injected neurons were treated by Taxol (0.1 μ M) or vinblastine (25 nM) for 20–30 min. Data represents ER crossings/10-μ m boundary length. Thirteen and 10 growth cones were assessed for Taxol and vinblastine treatments, respectively. Values are expressed as mean ± SEM. Statistical analysis by two-tailed paired *t* test. *$p < 0.001$ vs. before taxol or vinblastine addition.

ROS Derived from Rac1 Activation Facilitates 5-HT–evoked Ca^{2+} Release

The above-mentioned results are consistent with Rac1 effects on microtubule assembly promoting ER transport into the P-domain, thereby facilitating 5-HT–dependent Ca^{2+} release there. However, Rac effects on microtubule dynamics alone are not sufficient to explain our observations. Specifically, we noted that DN Rac1 abolished *all* 5-HT–dependent Ca^{2+} release in the growth cone (Figure 3F), including release in the C-domain where both microtubules and ER are clearly still present (Figure 1C).

Given that Rac is also an essential regulator of a multicomponent NADPH oxidase complex that controls ROS production (Lambeth, 2004) and recent evidence that cellular redox state can modulate Ca^{2+} release (Gordeeva *et al*., 2003; Davidson and Duchen, 2006), we decided to investigate the relationship between Rac1 activity, growth cone ROS levels, and 5-HT–evoked Ca^{2+} release.

To assess growth cone ROS activity, neurons were loaded with DCF, a live-cell fluorescent ROS detector (Xie *et al*., 1999). In control experiments, DCF levels corrected for volume were monitored during H_2O_2 exposure, and the response was obtained over time, confirming the sensitivity of DCF (Supplemental Figure S5). Next, ROS levels in different Rac1 backgrounds were quantified. CA Rac1 significantly increased baseline ROS levels in both C- and P-domains, whereas DN Rac1 had the opposite effect (Figure 6A). To test whether elevated baseline ROS levels in CA Rac1 backgrounds could be modulating Ca^{2+} mobilization, neurons were pretreated with an antioxidant NAC (Sundaresan *et al*., 1996; Suzukawa *et al*., 2000) and then exposed to 5-HT. Antioxidant pretreatment totally blocked 5-HT–evoked Ca^{2+} responses typical of CA Rac1-injected cells (Figure 6, B and F, and Supplemental Figure S6A; cf. Figure 3, C–E). Note that NAC (1 mM; 30 min) had no significant effect on ER distribution in growth cones (data not shown). Moreover, pretreatment of CA Rac1-injected neurons with apocynin, a specific inhibitor of NADPH oxidase complex assembly (Fellner and Arendshorst, 2005; Kimura *et al*., 2005), similarly suppressed 5-HT–evoked Ca^{2+} responses (Figure 6, C and F, and Supplemental Figure S6B). These data strongly suggest ROS derived from Rac1 dependent NADPH oxidase activation are necessary for Ca^{2+} responses to 5-HT in the entire growth cone, i.e., in either C- or P-domains.

If 5-HT–evoked Ca^{2+} release depends on the presence of ROS, exposure to exogenous ROS would be expected to rescue Ca^{2+} responses to 5-HT in DN Rac1 backgrounds. To

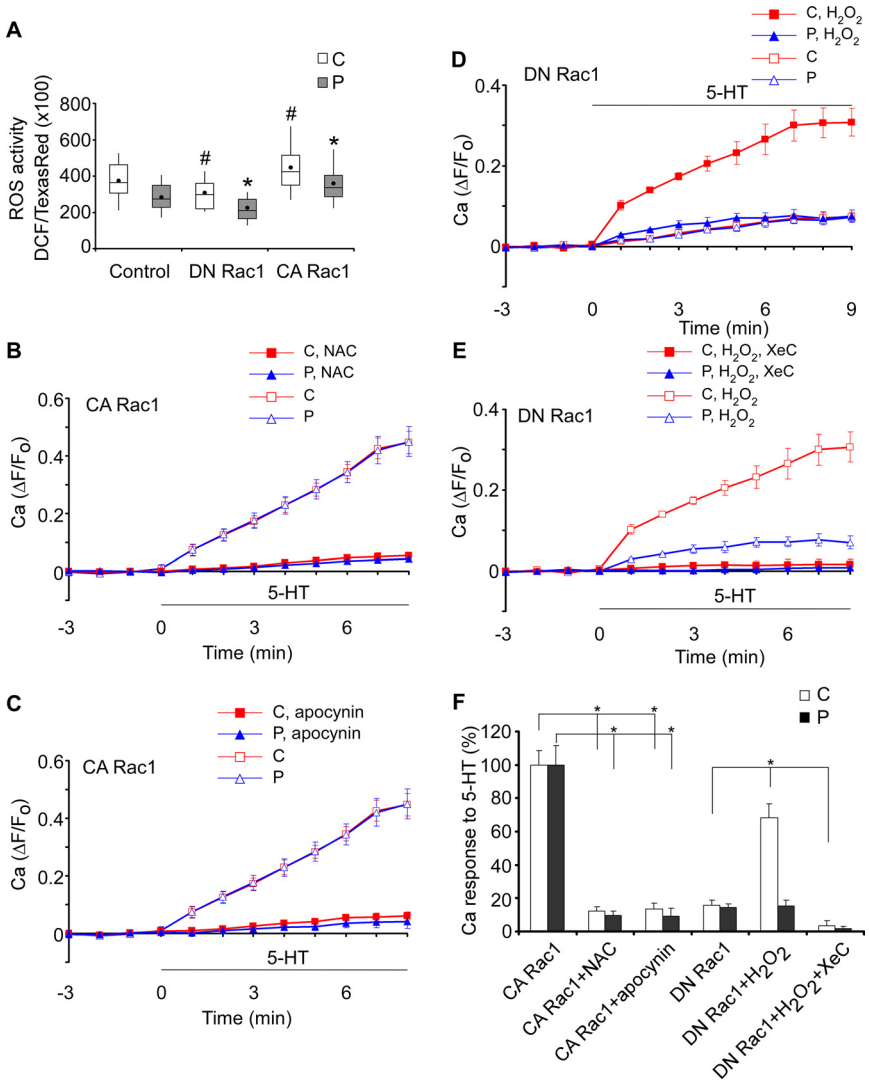

Figure 6. ROS derived from Rac1 activation promotes 5-HT–evoked Ca^{2+} response. (A) ROS levels measured in C- and P-domains in control, DN Rac1, or CA Rac1 backgrounds. N = 35 (control), 36 (DN Rac1), and 34 (CA Rac1). N denotes the number of growth cones tested. Values are expressed as whisker plots. Means are represented by dots, medians are represented by middle lines, 75th and 25th quartiles are represented by top and bottom of the boxes, respectively, and 90th and 10th percentiles are represented by whiskers. Statistical analysis by two tailed unpaired *t* test. #p < 0.05 and *p < 0.01 compared with control for C-domain and P-domain, respectively. (B and C) Summary of $\Delta F/F_0$ plots recorded in the entire C-domain (red sign) or P-domain (blue sign) of growth cones preincubated with NAC (1 mM, 20–30 min; B) or apocynin (1 mM, 40–50 min; C) to quantify Ca^{2+} response to 5-HT over time in CA Rac1 backgrounds. The control curves for C-domain and P-domain from Figure 3E are shown for comparison. N = 5 (CA Rac1 + NAC), 7 (CA Rac1 + apocynin), or 5 (CA Rac1). (D and E) Summary of $\Delta F/F_0$ plots recorded in the entire C-domain (red sign) or P-domain (blue sign) of growth cones pretreated with H_2O_2 (10 μM, 20–30 min; D) or H_2O_2 plus XeC (10 and 20 μM, respectively, 20–30 min; E) to quantify Ca^{2+} response to 5-HT over time in DN Rac1 backgrounds. The control curves for C-domain and P-domain from Figure 3G are shown in D, and the H_2O_2-conditioned curves for C-domain and P-domain from D are shown in E for comparison. N = 4 for each condition. N denotes the number of growth cones tested. Values are expressed as mean ± SEM. Black bar shows 5-HT presence. (F) Summary of 5-HT (10 μM)-evoked Ca^{2+} peak values presented in B–E. Data were obtained from the entire C-domain and P-domain and normalized to those in CA Rac1 conditions. Values are expressed as mean ± SEM. *p < 0.01.

test this hypothesis, cells injected with DN Rac1 were pretreated with a low concentration of H_2O_2, and Ca^{2+} responses were assessed. In sharp contrast to controls (Supplemental Figure S6C), addition of 5-HT to neurons conditioned with H_2O_2 (10 μM) resulted in dramatic Ca^{2+} increases in the C-domain (Figure 6, D and F, and Supplemental Fig. S6D). Ca^{2+} levels plateaued with a 30% increase after ~7 min in 5-HT (Figure 6D). H_2O_2 conditioning did not rescue Ca^{2+} responses in the P-domain (Figure 6, D and F, and Supplemental Figure S6D)—this is expected as a consequence of peripheral ER depletion in DN Rac1 backgrounds (Figure 1). Note that in DN Rac1 backgrounds, H_2O_2 (10 μM; 20 min) did not affect ER distribution in growth cones significantly (data not shown).

The H_2O_2 rescue responses mentioned above depended on IP_3 receptor activation, because Ca^{2+} release was absent in the presence of XeC (Figure 6, E and F, and Supplemental Figure S6E). In control or DN Rac1 injected neurons, H_2O_2 (10 μM) alone had little effect on growth cone morphology, and baseline Ca^{2+} levels did not change significantly (<5%) in the continued presence of H_2O_2 (>45 min exposure; data not shown). These results are consistent with a report that histamine-stimulated Ca^{2+} oscillations could be rescued in human aortic endothelial cells expressing DN Rac1, if cells were exposed to low concentration of H_2O_2 (Hu *et al.*, 2002). Together, these data suggest that Rac1 activity modulates 5-HT–evoked Ca^{2+} release via ROS-dependent sensitization of IP_3 receptors.

DISCUSSION

Given its signaling diversity, it is not surprising that Ca^{2+} dynamics are tightly regulated both spatially and temporally. Rac regulation of Ca^{2+} metabolism has been reported in other systems, for example, Rac/Cdc42-inactivating *clostridial cytotoxins* inhibited intracellular Ca^{2+} mobilization induced by FcεRI-stimulation in rat basophilic leukemia cells (Djouder *et al.*, 2000); CA Rac enhanced Ca^{2+} release from ER in mast cells after antigen stimulation, whereas DN Rac dampened Ca^{2+} mobilization (Hong-Geller and Cerione, 2000; Hong-Geller *et al.*, 2001). The current study extends the role of Rac in regulation of Ca^{2+} metabolism to neuronal growth cones, where 5-HT–evoked Ca^{2+} release topography, and sensitivity seems to be modulated by Rac1 activity via parallel effects on microtubule dynamics and IP_3 receptor sensitivity.

Microtubule-dependent Changes in the ER Ca^{2+} Store Distribution

Because intracellular Ca^{2+} stores reside in ER (Ross *et al*., 1989; Walton *et al*., 1991), which is a cargo for microtubule-based transport, Rac effects on microtubule dynamics could affect ER distribution. Indeed, Rac1 promotes microtubule growth in epithelial cells via Pac kinase-dependent inhibition of the microtubule catastrophe factor Op18/stathmin (Wittmann *et al*., 2004). Moreover, Rac activator DOCK7 inactivates Op18/stathmin in nascent axons (Watabe-Uchida *et al*., 2006). In agreement, we found that CA Rac1 facilitated microtubule extension into the P-domain by increasing microtubule rescue frequency and decreasing catastrophe frequency (Table 1). These effects were correlated with increased presence of microtubules and ER in the P-domain (Figures 1, A, B and E, and 2A). When microtubule assembly was disrupted by Taxol or vinblastine treatment (Figure 5A), ER was also cleared from the growth cone periphery (Table 2, Figure 5B, and Supplemental Figure S4C), resulting in attenuated 5-HT–evoked Ca^{2+} responses (Figure 5C and Supplemental Figure S4, A and B). Collectively, these data suggest that altering the spatial distribution of intracellular Ca^{2+} pools in the P-domain may be an important mechanism for modulating Ca^{2+} responses there.

We also found that paradoxically Taxol/vinblastine treatments attenuated Ca^{2+} responses to 5-HT in the C-domain (Figure 5C, 4 and 5, and Supplemental Figure S4B) and reduced ER density (Figure 5B and Supplemental Figure S4C) despite continued high microtubule density there (Figure 5A). These effects are interesting because they suggest the presence of a heretofore uncharacterized pool of dynamic microtubules in the C-domain that play a role in regulating ER distribution. Such a pool would be difficult to detect because the high density of microtubules in the C-domain precludes unambiguous analysis by speckle microscopy. These observations are consistent with a report that Taxol decreased thapsigargin-mediated Ca^{2+} release in adenocarcinoma cells (Padar *et al*., 2004). Note that neither Taxol (100 nM) nor vinblastine (25 nM) significantly altered basal Ca^{2+} levels in growth cones (data not shown), suggesting these pretreatments do not significantly perturb existing Ca^{2+} stores. It will be of interest to investigate these apparent microtubule assembly dependent effects on ER distribution in the C-domain in future studies.

In DN Rac1 backgrounds, microtubules and ER were still present in C-domain (Figure 1, A and C), but now 5-HT–dependent Ca^{2+} release was essentially absent (Figure 3, F and G). These data suggest that the Rac1 effects on microtubule assembly and ER transport discussed above are not sufficient to explain the potentiating effects of Rac activity on 5-HT–evoked Ca^{2+} responses. The role of Rac in ROS production seems to be the missing piece of this puzzle.

ROS-dependent Changes in Ca^{2+} Release

Rac plays an essential role in NADPH oxidase-mediated ROS production and related signaling (Lambeth, 2004; Bedard and Krause, 2007). Evidence suggests a close connection between Rac1 activation and ROS generation in a variety of cell types, including neurons (Suzukawa *et al*., 2000), liver cells (Cool *et al*., 1998), astroglioma cells (Lee *et al*., 2002), and fibroblasts (Sundaresan *et al*., 1996). Indeed, we found that CA Rac1 significantly increased ROS levels in the growth cone C- and P-domains, whereas DN Rac1 had the opposite effect (Figure 6A). Given that both IP_3 receptors and ryanodine receptors seem to be sensitized by ROS (Davidson and Duchen, 2006), elevated ROS levels we see in CA Rac1 backgrounds may facilitate 5-HT Ca^{2+} responses. In agreement, depleting ROS using a reactive oxygen scavenger (NAC) or blocking NADPH oxidase function (with apocynin) abolished 5-HT–evoked Ca^{2+} responses in CA Rac1 backgrounds (Figure 6, B, C, and F, and Supplemental Figure S6, A and B). In contrast, addition of extracellular H_2O_2 restored 5-HT–evoked Ca^{2+} release from IP_3 gated stores in DN Rac1 backgrounds (Figure 6, D, E, and F, and Supplemental Figure S6, D and E). These results support the idea that Rac1 activation is driving production of ROS that in turn potentiates the observed 5-HT–evoked Ca^{2+} responses. Parenthetically, treatment with the ROS scavenger

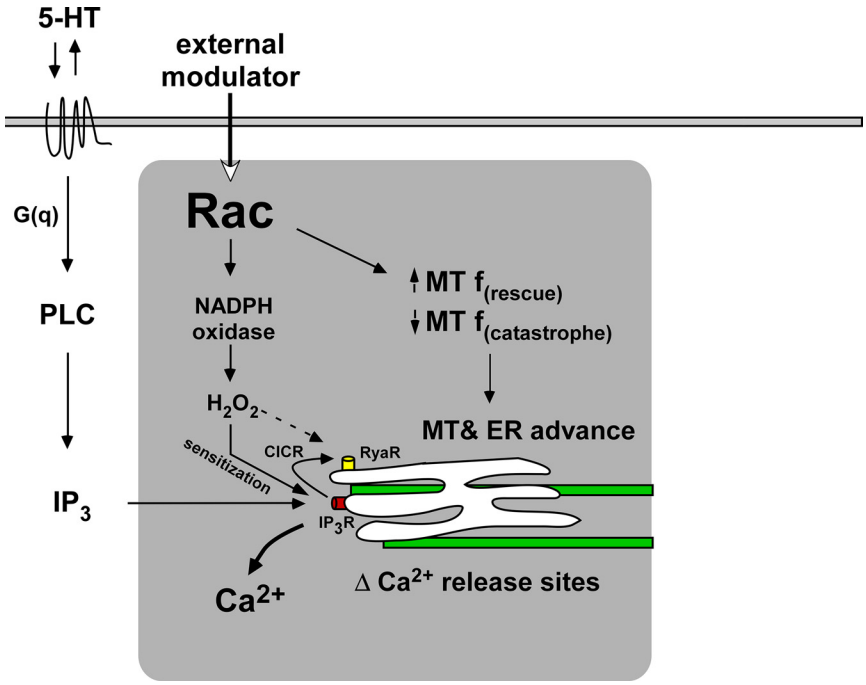

Figure 7. Model showing that Rac1 promotes 5-HT–induced Ca^{2+} mobilization by promoting microtubule-based ER advance and ROS-sensitized Ca^{2+} release. Rac-dependent Ca^{2+} regulation module is indicated by gray box. CICR, Ca^{2+} induced Ca^{2+} release.

NAC (1 mM; 30 min) or H_2O_2 (10 μM; 20 min) did not affect ER distribution (data not shown), consistent with segregation of Rac effects on microtubules and NADPH oxidase.

It is well known that ROS such as H_2O_2 inactivate protein tyrosine phosphatases by Cys oxidization and potentiate tyrosine kinase signaling (Tonks, 2005). It is unlikely that this plays a significant role here because pretreatment with genistein (100 μM), a general protein tyrosine kinase inhibitor, had no effect on H_2O_2 rescue of 5-HT–evoked Ca^{2+} responses in DN Rac1 backgrounds (data not shown). Because both IP_3 receptors and RyaRs are known to be sensitive to their thiol redox state, with oxidation of critical thiols favoring Ca^{2+} release (Abramson and Salama, 1988; Missiaen *et al*., 1991; Bootman *et al*., 1992; Xia *et al*., 2000; Joseph *et al*., 2006), we speculate that ROS may oxidize IP_3 and Rya receptors and thereby reduce the threshold for Ca^{2+} channel opening. Rac1 has also been reported to directly activate PLCβ (Illenberger *et al*., 1998; Snyder *et al*., 2003); however, we do not think constitutive PLC activation is involved because 1) Ca^{2+} responses were rescued by H_2O_2 in DN Rac1 backgrounds (Figure 6, D and F, and Supplemental Figure S6D) and 2) Ca^{2+} responses still depended on IP_3 receptor activation (Figure 6, E and F, and Supplemental Fig. S6E).

Rac is emerging as a functional node for coordination of multiple biochemical processes (Figure 7); here, we add to this story by providing evidence that Rac "modulates" the topology and sensitivity of Ca^{2+} release by 1) regulating microtubule assembly, which in turn affects ER distribution; and 2) increasing ROS production, which leads to sensitization of evoked Ca^{2+} release from IP_3-dependent stores. Although Rac activation would create an environment that facilitates stimuli-evoked Ca^{2+} responses, it is difficult to predict the relative importance of Rac effects stemming from changes in microtubule dynamics versus ROS production because each of these processes could be influenced by other signaling pathways.

Ca^{2+} diffusion is highly restricted by binding proteins and pumps (Augustine *et al*., 2003); thus, downstream effectors in growth cones need to be situated relatively close to sites of Ca^{2+} release. We speculate that localized regions of high Rac activity will tend to accumulate microtubules due to net effects on assembly, this in turn will bring ER stores into proximity with potential Ca^{2+} effector proteins. Positive external modulators of Rac activity could thus "prime" the P-domain for ligand-dependent Ca^{2+} release (Figure 7). In primed regions, ligand dependent responses involving the PLC$\rightarrow IP_3$ cascade would also be facilitated by increased ROS levels. The net result would be a spatio-temporal sensitization of ligand dependent Ca^{2+} responses. The dependence of 5-HT–evoked Ca^{2+} responses on Rac activity presented here are in line with this type of model. It will be of interest to see how these Rac dependent processes affect the cytoskeletal proteins dynamics involved in axon growth.

ACKNOWLEDGMENTS

We thank Forscher laboratory members for insightful discussion of this work, Dr. Andrew Schaefer in particular for help in assessing microtubule dynamics, and David van Goor for suggestions on Ca^{2+} data analysis. This work was supported by National Institutes of Health grants R01-NS28695 and R01-NS051786 (to P. F.) and the Nikon Partners-in-Research Program.

REFERENCES

Abramson, J. J., and Salama, G. (1988). Sulfhydryl oxidation and Ca2+ release from sarcoplasmic reticulum. Mol. Cell Biochem. *82*, 81–84.

Augustine, G. J., Santamaria, F., and Tanaka, K. (2003). Local calcium signaling in neurons. Neuron *40*, 331–346.

Barbas, D., Campbell, A., Castellucci, V. F., and DesGroseillers, L. (2005). Comparative localization of two serotonin receptors and sensorin in the central nervous system of *Aplysia* californica. J. Comp. Neurol. *490*, 295–304.

Bedard, K., and Krause, K. H. (2007). The NOX family of ROS-generating NADPH oxidases: physiology and pathophysiology. Physiol. Rev. *87*, 245–313.

Bedlack, R. S., Jr., Wei, M., and Loew, L. M. (1992). Localized membrane depolarizations and localized calcium influx during electric field-guided neurite growth. Neuron *9*, 393–403.

Bootman, M. D., Taylor, C. W., and Berridge, M. J. (1992). The thiol reagent, thimerosal, evokes Ca^{2+} spikes in HeLa cells by sensitizing the inositol 1,4,5-trisphosphate receptor. J. Biol. Chem. *267*, 25113–25119.

Cheng, S., Geddis, M. S., and Rehder, V. (2002). Local calcium changes regulate the length of growth cone filopodia. J. Neurobiol. *50*, 263–275.

Chiu, C. T., Tsao, H. L., Fan, L. W., Wang, C. C., Chien, C. S., and Yang, C. M. (1999). 5-Hydroxytryptamine-induced phosphoinositide hydrolysis and Ca2+ mobilisation in canine cultured aorta smooth muscle cells. Cell Signal. *11*, 361–370.

Cifuentes, F., Gonzalez, C. E., Fiordelisio, T., Guerrero, G., Lai, F. A., and Hernandez-Cruz, A. (2001). A ryanodine fluorescent derivative reveals the presence of high-affinity ryanodine binding sites in the Golgi complex of rat sympathetic neurons, with possible functional roles in intracellular Ca(2+) signaling. Cell Signal. *13*, 353–362.

Cohan, C. S., Connor, J. A., and Kater, S. B. (1987). Electrically and chemically mediated increases in intracellular calcium in neuronal growth cones. J. Neurosci. *7*, 3588–3599.

Cohan, C. S., and Kater, S. B. (1986). Suppression of neurite elongation and growth cone motility by electrical activity. Science *232*, 1638–1640.

Connor, J. A. (1986). Digital imaging of free calcium changes and of spatial gradients in growing processes in single, mammalian central nervous system cells. Proc. Natl. Acad. Sci. USA *83*, 6179–6183.

Cool, R. H., Merten, E., Theiss, C., and Acker, H. (1998). Rac1, and not Rac2, is involved in the regulation of the intracellular hydrogen peroxide level in HepG2 cells. Biochem. J. *332*, 5–8.

Dailey, M. E., and Bridgman, P. C. (1989). Dynamics of the endoplasmic reticulum and other membranous organelles in growth cones of cultured neurons. J. Neurosci. *9*, 1897–1909.

Dailey, M. E., and Bridgman, P. C. (1991). Structure and organization of membrane organelles along distal microtubule segments in growth cones. J. Neurosci. Res. *30*, 242–258.

Davidson, S. M., and Duchen, M. R. (2006). Calcium microdomains and oxidative stress. Cell Calcium *40*, 561–574.

Deng, Y., Bennink, J. R., Kang, H. C., Haugland, R. P., and Yewdell, J. W. (1995). Fluorescent conjugates of brefeldin A selectively stain the endoplasmic reticulum and Golgi complex of living cells. J. Histochem. Cytochem. *43*, 907–915.

Djouder, N., Prepens, U., Aktories, K., and Cavalie, A. (2000). Inhibition of calcium release-activated calcium current by Rac/Cdc42-inactivating clostridial cytotoxins in RBL cells. J. Biol. Chem. *275*, 18732–18738.

Dropic, A. J., Brailoiu, E., and Cooper, R. L. (2005). Presynaptic mechanism of action induced by 5-HT in nerve terminals: possible involvement of ryanodine and IP3 sensitive 2+ stores. Comp. Biochem. Physiol. A Mol. Integr. Physiol. *142*, 355–361.

Etienne-Manneville, S., and Hall, A. (2002). Rho GTPases in cell biology. Nature *420*, 629–635.

Fellner, S. K., and Arendshorst, W. J. (2005). Angiotensin II, reactive oxygen species, and Ca2+ signaling in afferent arterioles. Am. J. Physiol. Renal Physiol. *289*, F1012–F1019.

Fleming, I. N., Elliott, C. M., Buchanan, F. G., Downes, C. P., and Exton, J. H. (1999). Ca2+/calmodulin-dependent protein kinase II regulates Tiam1 by reversible protein phosphorylation. J. Biol. Chem. *274*, 12753–12758.

Forscher, P., Kaczmarek, L. K., Buchanan, J. A., and Smith, S. J. (1987). Cyclic AMP induces changes in distribution and transport of organelles within growth cones of *Aplysia* bag cell neurons. J. Neurosci. *7*, 3600–3611.

Gafni, J., Munsch, J. A., Lam, T. H., Catlin, M. C., Costa, L. G., Molinski, T. F., and Pessah, I. N. (1997). Xestospongins: potent membrane permeable blockers of the inositol 1,4,5-trisphosphate receptor. Neuron *19*, 723–733.

Garyantes, T. K., and Regehr, W. G. (1992). Electrical activity increases growth cone calcium but fails to inhibit neurite outgrowth from rat sympathetic neurons. J. Neurosci. *12*, 96–103.

Gaspar, P., Cases, O., and Maroteaux, L. (2003). The developmental role of serotonin: news from mouse molecular genetics. Nat. Rev. Neurosci. *4*, 1002–1012.

Gomez, T. M., Robles, E., Poo, M., and Spitzer, N. C. (2001). Filopodial calcium transients promote substrate-dependent growth cone turning. Science *291*, 1983–1987.

Gomez, T. M., Snow, D. M., and Letourneau, P. C. (1995). Characterization of spontaneous calcium transients in nerve growth cones and their effect on growth cone migration. Neuron *14*, 1233–1246.

Gomez, T. M., and Spitzer, N. C. (1999). In vivo regulation of axon extension and pathfinding by growth-cone calcium transients. Nature *397*, 350–355.

Gomez, T. M., and Zheng, J. Q. (2006). The molecular basis for calcium-dependent axon pathfinding. Nat. Rev. Neurosci. *7*, 115–125.

Gordeeva, A. V., Zvyagilskaya, R. A., and Labas, Y. A. (2003). Cross-talk between reactive oxygen species and calcium in living cells. Biochemistry *68*, 1077–1080.

Grigoriev, I., *et al*. (2008). STIM1 is a MT-plus-end-tracking protein involved in remodeling of the ER. Curr. Biol. *18*, 177–182.

Guan, K. L., and Rao, Y. (2003). Signalling mechanisms mediating neuronal responses to guidance cues. Nat. Rev. Neurosci. *4*, 941–956.

Hall, A. (1998). Rho GTPases and the actin cytoskeleton. Science *279*, 509–514.

Henley, J., and Poo, M. M. (2004). Guiding neuronal growth cones using Ca2+ signals. Trends Cell Biol. *14*, 320–330.

Hong-Geller, E., and Cerione, R. A. (2000). Cdc42 and Rac stimulate exocytosis of secretory granules by activating the IP(3)/calcium pathway in RBL-2H3 mast cells. J. Cell Biol. *148*, 481–494.

Hong-Geller, E., Holowka, D., Siraganian, R. P., Baird, B., and Cerione, R. A. (2001). Activated Cdc42/Rac reconstitutes Fcepsilon RI-mediated Ca2+ mobilization and degranulation in mutant RBL mast cells. Proc. Natl. Acad. Sci. USA *98*, 1154–1159.

Hu, Q., Yu, Z. X., Ferrans, V. J., Takeda, K., Irani, K., and Ziegelstein, R. C. (2002). Critical role of NADPH oxidase-derived reactive oxygen species in generating Ca2+ oscillations in human aortic endothelial cells stimulated by histamine. J. Biol. Chem. *277*, 32546–32551.

Illenberger, D., Schwald, F., Pimmer, D., Binder, W., Maier, G., Dietrich, A., and Gierschik, P. (1998). Stimulation of phospholipase C-beta2 by the Rho GTPases Cdc42Hs and Rac1. EMBO J. *17*, 6241–6249.

Jaffe, A. B., and Hall, A. (2005). Rho GTPases: biochemistry and biology. Annu. Rev. Cell Dev. Biol. *21*, 247–269.

Jin, M., Guan, C. B., Jiang, Y. A., Chen, G., Zhao, C. T., Cui, K., Song, Y. Q., Wu, C. P., Poo, M. M., and Yuan, X. B. (2005). Ca2+-dependent regulation of rho GTPases triggers turning of nerve growth cones. J. Neurosci. *25*, 2338–2347.

Jin, W., Lo, T. M., Loh, H. H., and Thayer, S. A. (1994). U73122 inhibits phospholipase C-dependent calcium mobilization in neuronal cells. Brain Res. *642*, 237–243.

Joseph, S. K., Nakao, S. K., and Sukumvanich, S. (2006). Reactivity of free thiol groups in type-I inositol trisphosphate receptors. Biochem. J. *393*, 575–582.

Kimura, S., Zhang, G. X., Nishiyama, A., Shokoji, T., Yao, L., Fan, Y. Y., Rahman, M., Suzuki, T., Maeta, H., and Abe, Y. (2005). Role of NAD(P)H oxidase- and mitochondria-derived reactive oxygen species in cardioprotection of ischemic reperfusion injury by angiotensin II. Hypertension *45*, 860–866.

Lambeth, J. D. (2004). NOX enzymes and the biology of reactive oxygen. Nat. Rev. Immunol. *4*, 181–189.

Lau, P. M., Zucker, R. S., and Bentley, D. (1999). Induction of filopodia by direct local elevation of intracellular calcium ion concentration. J. Cell Biol. *145*, 1265–1275.

Lee, M., You, H. J., Cho, S. H., Woo, C. H., Yoo, M. H., Joe, E. H., and Kim, J. H. (2002). Implication of the small GTPase Rac1 in the generation of reactive oxygen species in response to beta-amyloid in C6 astroglioma cells. Biochem. J. *366*, 937–943.

Li, Q., Roberts, A. C., and Glanzman, D. L. (2005). Synaptic facilitation and behavioral dishabituation in *Aplysia*: dependence on release of Ca2+ from postsynaptic intracellular stores, postsynaptic exocytosis, and modulation of postsynaptic AMPA receptor efficacy. J. Neurosci. *25*, 5623–5637.

Li, X. C., Giot, J. F., Kuhl, D., Hen, R., and Kandel, E. R. (1995). Cloning and characterization of two related serotonergic receptors from the brain and the reproductive system of *Aplysia* that activate phospholipase C. J. Neurosci. *15*, 7585–7591.

Lin, C. H., and Forscher, P. (1995). Growth cone advance is inversely proportional to retrograde F-actin flow. Neuron *14*, 763–771.

Luo, L. (2000). Rho GTPases in neuronal morphogenesis. Nat. Rev. Neurosci. *1*, 173–180.

Mattson, M. P., and Kater, S. B. (1987). Calcium regulation of neurite elongation and growth cone motility. J. Neurosci. *7*, 4034–4043.

McPherson, P. S., Kim, Y. K., Valdivia, H., Knudson, C. M., Takekura, H., Franzini-Armstrong, C., Coronado, R., and Campbell, K. P. (1991). The brain ryanodine receptor: a caffeine-sensitive calcium release channel. Neuron *7*, 17–25.

Meissner, G. (1986). Ryanodine activation and inhibition of the Ca2+ release channel of sarcoplasmic reticulum. J. Biol. Chem. *261*, 6300–6306.

Missiaen, L., Taylor, C. W., and Berridge, M. J. (1991). Spontaneous calcium release from inositol trisphosphate-sensitive calcium stores. Nature *352*, 241–244.

Munro, S., and Pelham, H. R. (1987). A C-terminal signal prevents secretion of luminal ER proteins. Cell *48*, 899–907.

Noda, M., *et al*. (2003). Recombinant human serotonin 5A receptors stably expressed in C6 glioma cells couple to multiple signal transduction pathways. J. Neurochem. *84*, 222–232.

Padar, S., van Breemen, C., Thomas, D. W., Uchizono, J. A., Livesey, J. C., and Rahimian, R. (2004). Differential regulation of calcium homeostasis in adenocarcinoma cell line A549 and its Taxol-resistant subclone. Br. J. Pharmacol. *142*, 305–316.

Price, L. S., Langeslag, M., ten Klooster, J. P., Hordijk, P. L., Jalink, K., and Collard, J. G. (2003). Calcium signaling regulates translocation and activation of Rac. J. Biol. Chem. *278*, 39413–39421.

Ross, C. A., Meldolesi, J., Milner, T. A., Satoh, T., Supattapone, S., and Snyder, S. H. (1989). Inositol 1,4,5-trisphosphate receptor localized to endoplasmic reticulum in cerebellar Purkinje neurons. Nature *339*, 468–470.

Saunders, C., and Cohen, R. S. (1999). The role of oocyte transcription, the 5′UTR, and translation repression and derepression in *Drosophila* gurken mRNA and protein localization. Mol. Cell *3*, 43–54.

Schaefer, A. W., Kabir, N., and Forscher, P. (2002). Filopodia and actin arcs guide the assembly and transport of two populations of microtubules with unique dynamic parameters in neuronal growth cones. J. Cell Biol. *158*, 139–152.

Smith, R. J., Sam, L. M., Justen, J. M., Bundy, G. L., Bala, G. A., and Bleasdale, J. E. (1990). Receptor-coupled signal transduction in human polymorphonuclear neutrophils: effects of a novel inhibitor of phospholipase C-dependent processes on cell responsiveness. J. Pharmacol. Exp. Ther. *253*, 688–697.

Snyder, J. T., Singer, A. U., Wing, M. R., Harden, T. K., and Sondek, J. (2003). The pleckstrin homology domain of phospholipase C-beta2 as an effector site for Rac. J. Biol. Chem. *278*, 21099–21104.

Solovyova, N., and Verkhratsky, A. (2003). Neuronal endoplasmic reticulum acts as a single functional Ca2+ store shared by ryanodine and inositol-1,4,5-trisphosphate receptors as revealed by intra-ER [Ca2+] recordings in single rat sensory neurones. Pflugers Arch *446*, 447–454.

Sundaresan, M., Yu, Z. X., Ferrans, V. J., Sulciner, D. J., Gutkind, J. S., Irani, K., Goldschmidt-Clermont, P. J., and Finkel, T. (1996). Regulation of reactive-oxygen-species generation in fibroblasts by Rac1. Biochem. J. *318*, 379–382.

Suter, D. M., Schaefer, A. W., and Forscher, P. (2004). Microtubule dynamics are necessary for SRC family kinase-dependent growth cone steering. Curr. Biol. *14*, 1194–1199.

Suzukawa, K., Miura, K., Mitsushita, J., Resau, J., Hirose, K., Crystal, R., and Kamata, T. (2000). Nerve growth factor-induced neuronal differentiation requires generation of Rac1-regulated reactive oxygen species. J. Biol. Chem. *275*, 13175–13178.

Takei, K., Shin, R. M., Inoue, T., Kato, K., and Mikoshiba, K. (1998). Regulation of nerve growth mediated by inositol 1,4,5-trisphosphate receptors in growth cones. Science *282*, 1705–1708.

Terasaki, M., Chen, L. B., and Fujiwara, K. (1986). Microtubules and the endoplasmic reticulum are highly interdependent structures. J. Cell Biol. *103*, 1557–1568.

Tonks, N. K. (2005). Redox redux: revisiting PTPs and the control of cell signaling. Cell *121*, 667–670.

Walton, P. D., Airey, J. A., Sutko, J. L., Beck, C. F., Mignery, G. A., Sudhof, T. C., Deerinck, T. J., and Ellisman, M. H. (1991). Ryanodine and inositol trisphosphate receptors coexist in avian cerebellar Purkinje neurons. J. Cell Biol. *113*, 1145–1157.

Watabe-Uchida, M., John, K. A., Janas, J. A., Newey, S. E., and Van Aelst, L. (2006). The Rac activator DOCK7 regulates neuronal polarity through local phosphorylation of stathmin/Op18. Neuron *51*, 727–739.

Waterman-Storer, C. M., Desai, A., Bulinski, J. C., and Salmon, E. D. (1998). Fluorescent speckle microscopy, a method to visualize the dynamics of protein assemblies in living cells. Curr. Biol. *8*, 1227–1230.

Waterman-Storer, C. M., and Salmon, E. D. (1998a). Endoplasmic reticulum membrane tubules are distributed by microtubules in living cells using three distinct mechanisms. Curr. Biol. *8*, 798–806.

Waterman-Storer, C. M., and Salmon, E. D. (1998b). How microtubules get fluorescent speckles. Biophys. J. *75*, 2059–2069.

Wittmann, T., Bokoch, G. M., and Waterman-Storer, C. M. (2003). Regulation of leading edge microtubule and actin dynamics downstream of Rac1. J. Cell Biol. *161*, 845–851.

Wittmann, T., Bokoch, G. M., and Waterman-Storer, C. M. (2004). Regulation of microtubule destabilizing activity of Op18/stathmin downstream of Rac1. J. Biol. Chem. *279*, 6196–6203.

Xia, R., Stangler, T., and Abramson, J. J. (2000). Skeletal muscle ryanodine receptor is a redox sensor with a well defined redox potential that is sensitive to channel modulators. J. Biol. Chem. *275*, 36556–36561.

Xie, Z., Kometiani, P., Liu, J., Li, J., Shapiro, J. I., and Askari, A. (1999). Intracellular reactive oxygen species mediate the linkage of Na+/K+-ATPase to hypertrophy and its marker genes in cardiac myocytes. J. Biol. Chem. *274*, 19323–19328.

Yoder, E. J., Tamir, H., and Ellisman, M. H. (1996). 5-Hydroxytryptamine2A receptors on cultured rat Schwann cells. Glia *17*, 15–27.

Zhang, X. F., Schaefer, A. W., Burnette, D. T., Schoonderwoert, V. T., and Forscher, P. (2003). Rho-dependent contractile responses in the neuronal growth cone are independent of classical peripheral retrograde actin flow. Neuron *40*, 931–944.

Zhou, W. L., Sugioka, M., and Yamashita, M. (1999). Lysophosphatidic acid-induced Ca(2+) mobilization in the neural retina of chick embryo. J. Neurobiol. *41*, 495–504.